Orbital Mott transition in two dimensional pyrochlore lattice

Abhinav Saket[1] and Rajarshi Tiwari[2,3]

[1] Samastipur College, Samastipur, Bihar-848134, India
[2] School of Physics and CRANN, Trinity College, Dublin 2, Ireland

E-mail: rajarshi84@gmail.com

CrossMark

Abstract

We study orbital Mott transition in two dimensional pyrochlore lattice, using a two orbital Hubbard model with only inter-orbital electronic hopping. We use a real space Monte Carlo based approach to study the model at finite temperature, and establish temperature-interaction phase diagram that highlights the Mott transition, orbital ordering, and spectral trends, and possible window of pseudogap. Due to only inter-orbital hopping, the Mott insulator 'generates' ferro exchange resulting in ferro-orbital ordering, with T_{corr}/t peaked at ≈ 0.2 around $U/t \approx 6$. The optical conductivity shows unusual two peak feature due to two dimensional pyrochlore lattice.

(Some figures may appear in colour only in the online journal)

1. Introduction

The Mott transition is one of the most widely discussed phenomenon in strongly correlated systems [1, 2]. It manifests itself at 'integer' filling when electrons localise due to electron–electron interaction, resulting in an insulating state, called Mott insulator. The 'Mott problem', i.e., understanding why the transition occurs and its consequences, is most commonly studied through single band Hubbard model [3] on different lattices. The addition of orbital degrees of freedom opens more exciting possibilities, such as interplay of orbital and spin degrees of freedom [4], orbital selective Mott transition [5], where some orbitals localise, while other remain itinerant. These possibilities, are, however, explored at the cost of more complex models that include intra and inter orbital repulsions and exchange energies [6]. Formally, each energy scale/parameter adds a dimension to the parameter space, making it harder to comprehend. As a result, studies geared towards model solving usually reduce the parameter space, by assuming simpler electronic hopping structure, and choosing reduced set of interactions, such as absence of inter-orbital repulsion [7], fixing interaction to some representative values [8, 9], or

choosing same intra and inter-orbital repulsions by removing Hund's coupling [10].

To solve the Hubbard model for finite temperature, DMFT has been a method of choice, be it single orbital model [11, 12], or multi-orbital model [7, 8, 13]. Many qualitative features of orbital-degenerate Mott transition are found to be available in single band model as well [13], however new features emerge, that require non-trivial treatment of multiple orbitals, such as different scaling of the critical couplings U_{c1} and U_{c2} as function of the number of orbitals [7]. Recently, Kawakami *et al* studied the Mott transition in the three-orbital Hubbard model and investigated how the orbital level splitting affects the Mott transition in the case of two electrons per site using (DMFT) combined with continuous-time quantum Monte Carlo simulations [8]. A general mechanism for the coexistence of both itinerant and localised conduction electrons has been proposed [14] and the orbital selective Mott transition in two-band Hubbard models with different bandwidths has been explored using another form of DMFT [15].

Within DMFT, or its cluster variants [16, 17], the correlated lattice system is mapped to one or more correlated sites coupled with non-interacting bath of electrons, and one gets to solve the quantum problem at the cost of ignoring spatial fluctuation in the lattice. The neglect of spatial correlations and

the lack of visual intuition about the transition, motivated us in past to explore a complementary real-space Monte Carlo based approach (discussed later), which provides a reasonable description of Mott physics in a real space setting and allows a certain degree of visualization.

In this paper, we use this approach to solve a two orbital Hubbard model, inspired from the recent interest in pyrochlore compounds for studying the effects of spin–orbital interplay and geometrical frustration [18]. The metal-insulator transition (MIT) in Mo pyrochlore oxides ($R_2Mo_2O_7$) [19] (where R is rare earth metal) and role of its frustrated lattice structure has been extensively studied earlier for Ir based pyrochlore [20, 21]. The evolution of charge dynamics at metal-insulator transition has been experimentally investigated for $Nd_2(Ir_{1-x}Rh_x)_2O_7$ where the spin–orbit interaction as well as the electron correlation is effectively tuned by the doping level x [22]. The transition from ferromagnetic metal to spin glass insulator and paramagnetic metal has been observed with increase of the radius of rare earth metal ion R^{3+} and external pressure due to the competing double exchange and super exchange interactions on the frustrated lattice [23]. Likewise, the role of orbital degrees of freedom has been debated in metal insulator transitions in various pyrochlore oxides [24].

A number of theoretical attempts have been made to explore the antiferromagnetism [25], frustration [26–28], Hall effect [29] etc, through a variety of models. Ground state [19] and finite temperature phase diagrams [30] have been established, showing transition from ferromagnetic to spin glass, or cooperative paramagnetic phase. However, these transitions are seen primarily in terms of double-exchange model without electron–electron interaction, or within weak interaction limit. Furukawa *et al* [19] (figure 2) illustrated an elegant schematic of phases in terms of interaction and super-exchange phase diagram, which shows the possibility of orbital Mott transition in the ferromagnetic spin background in the weak super-exchange limit. We wish to explore this transition in detail.

2. Model

The lattice structure of $R_2Mo_2O_7$ is composed of two intervening pyrochlore lattices formed by Mo cations and R cations. The Mo cation is surrounded by octahedra of oxygens (MoO_6), which splits the five fold degenerate d-orbitals into three and two fold degenerate t_{2g} and e_g orbitals respectively. Further, the distortion of the MoO_6 octahedra along local (111) axis (towards centre of each Mo tetrahedra) splits the t_{2g} levels into lower single a_{1g} level (below Fermi level) and higher two fold degenerate e'_g levels (above Fermi level) [31]. Mo being Mo^{4+} cation in these compounds, strong Hund's coupling results in the fully occupied single a_{1g} up-spin band, well below Fermi level, and half-filled two-fold degenerate e'_g up-spin bands. We start with the following two band double exchange model, previously proposed by Furukawa *et al* [19] for various pyrochlore systems to describe the electronic motion for the compound, including kinetic energy, coulomb interaction, Hund's coupling and anti-ferromagnetic super-exchange:
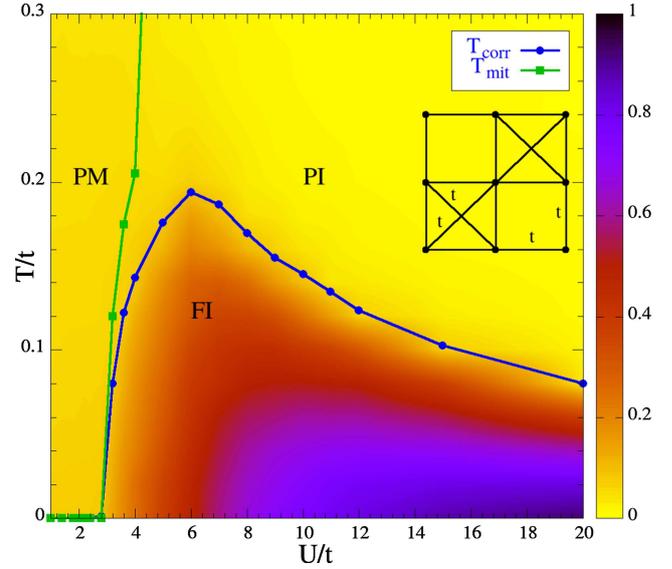
Figure 1. The phase diagram of the Furukawa model on checkerboard lattice (shown in the inset) in the $U/t, T/t$ plane. The colour map denotes the value of maxima of $S(\mathbf{q})$ at given temperature and U/t. The maxima in this case corresponds to $\mathbf{q} = (0, 0)$, which gives the ferromagnetic order. The blue (circle) curve shows T_{corr} temperature, at which magnetic correlation grow up to lattice size. The green (square) curve shows the metal-insulator transition, determined by the sign of $d\rho/dT$ (see text).

$$H = - \sum_{\langle ij\rangle, \alpha\beta\sigma} t_{\alpha\beta} \left(c^\dagger_{i\alpha\sigma} c_{j\beta\sigma} + \text{h.c.} \right) + J_H \sum_{i\alpha} \vec{S}_i \cdot \vec{s}_{i,\alpha}$$

$$+ \sum_{i\alpha\beta\alpha'\beta'\sigma\sigma'} U_{\alpha\beta\alpha'\beta'} c^\dagger_{i\alpha\sigma} c^\dagger_{i\beta\sigma'} c_{i\beta'\sigma'} c_{i\alpha'\sigma}$$

$$+ J_{AF} \sum_{\langle ij\rangle} \vec{S}_i \cdot \vec{S}_j \tag{1}$$

where, $c^\dagger_{i\alpha\sigma}$ creates an electron at site i, orbital α and spin σ. $\vec{s}_{i\alpha}$ is electronic spin operator for site i, orbital α. $\vec{S}_i$ is core spin at site i. The first term denotes the kinetic energy of itinerant e'_g electrons with spin σ and orbitals α running over two degenerate orbitals (say 1, and 2) of the e'_g band. $t_{\alpha,\beta}$ is the electronic hopping. Second term, with coupling J_H, denotes double exchange coupling between itinerant e'_g electrons with localised a_{1g} electron, treated as core spins. Third term denotes the anti-ferromagnetic super-exchange among localised a_{1g} electrons with strength J_{AF}. $J_{AF} =$ is approximately set by t^2_{a1g}/U_{a1g} where t_{a1g} is the transfer integral between the a_{1g} orbitals and U_{a1g} the intra-orbital Coulomb repulsion in the a_{1g} orbital. The last term denotes on-site coulomb interactions between e'_g including intra and inter-orbital repulsions.

We study the above two band double exchange (DE) model (1) on the two dimensional pyrochlore lattice, which is essentially 'checkerboard lattice' (shown in the inset of figure 1), in the limit $J_{AF} = 0$. This gets further simplified in the $J_H \to \infty$ limit as follow. Rotating the axis of quantization of every fermionic operator $c_{i,\alpha}$ from universal z-axis to the direction of the core spin $S_i(\theta_i, \phi_i)$ at every site,

$$\begin{bmatrix} c_{i,\uparrow} \\ c_{i,\downarrow} \end{bmatrix} = U(\theta_i, \phi_i) \begin{bmatrix} p_i \\ a_i \end{bmatrix} \quad \text{where}$$

$$U(\theta_i, \phi_i) = \exp\left(-i\frac{\phi_i}{2}\sigma^z\right) \exp\left(-i\frac{\theta_i}{2}\sigma^y\right). \quad (2)$$

renders the Hund's term diagonal in spin, and in $J_H \to \infty$ limit, the parallel p_i state gets projected out from the Hamiltonian, as have higher energy. By shifting the zero of the energy by J_H, we get the following low energy Hamiltonian, written in terms of the a_i operators with their axes aligned opposite to the localised spin at each site [19].

$$H = -\sum_{\langle ij\rangle\alpha\beta} t_{i\alpha,j\beta}\left(a_{i\alpha}^\dagger a_{j\beta} + \text{h.c.}\right) + U\sum_{i,\alpha\neq\beta} n_{i\alpha}n_{i\beta} \quad (3)$$

where $a_{i\alpha}$ is spinless fermion operator and $n_{i\alpha} = a_{i\alpha}^\dagger a_{i\alpha}$. U is inter-orbital interaction and the electronic hopping element $t_{i\alpha,j\beta}$ becomes angle dependent, (θ_i, ϕ_i) being the angles of spin $\vec{S}_i$.

$$t_{i\alpha,j\beta} = t_{\alpha\beta}\left(\cos\frac{\theta_i}{2}\cos\frac{\theta_j}{2} + e^{i(\phi_i-\phi_j)}\sin\frac{\theta_i}{2}\sin\frac{\theta_j}{2}\right) \quad (4)$$

Its easy to see from equation (4) that $t_{i\alpha,j\beta} = t_{\alpha,\beta}$ if the spins are parallel ($\theta_i = \theta_j, \phi_i = \phi_j$), and $t_{i\alpha,j\beta} = 0$ when they are anti-parallel ($\theta_i = \pi - \theta_j, \phi_i = \pi + \phi_j$). Thus, for $t_{i,j}$ to be maximum, nearest neighbouring spins have to be parallel to each other. In general, a non-trivial core spin state would generate complex spatial texture of hopping for electrons to delocalise. However, since we consider $J_{AF} = 0$, the ground state for the core spins is ferromagnetic (FM), with its T_c driven by the kinetic energy, which we assume to be large compared to $\sim t_{ij}^2/U$, so we can approximate the the core spins to be frozen in FM state, for which the hopping becomes site independent $t_{i\alpha,j\beta} = t_{\alpha\beta}$. We comment more on this later during the discussion.

Because of anisotropy of the e'_g orbitals and relative angle of Mo–O–Mo bond [19, 32], the relative strength of $t_{\alpha=\beta}$ and $t_{\alpha\neq\beta}$ can be expressed as [19] $\frac{t_{\alpha\neq\beta}}{t_{\alpha=\beta}} = \frac{3-\cos\delta}{3+\cos\delta}$. In Mo pyrochlore oxides $\delta > 90°$, and in Mo based systems about 130° [33] so the inter orbital hopping $t_{\alpha\neq\beta}$ is larger than the intra orbital hopping $t_{\alpha=\beta}$ [19]. So we choose, for simplicity, $t_{\alpha=\beta} = 0$, and set $t_{\alpha\neq\beta} = t$. We will comment on the inclusion of the intra-orbital hopping in the section 4.

Treating the two orbital as 'pseudo-spins' $\uparrow, \downarrow$, we get the following 'orbital-Hubbard model':

$$H = -t\sum_{\langle ij\rangle}\left(a_{i\uparrow}^\dagger a_{j\downarrow} + a_{i\downarrow}^\dagger a_{j\uparrow} + \text{h.c.}\right) + U\sum_i n_{i\uparrow}n_{i\downarrow} \quad (5)$$

Notice that, in this model, electrons delocalise through hopping alternatively via the two 'pseudo-spin' channels, which, as opposed to the usual Hubbard model, would generate 'ferromagnetic' interaction among the neighbouring pseudo-spins in large U/t Mott state, because due to the presence of 'alternate hopping', an electron of spin $\uparrow$ at site i can virtually hop to neighbouring site j and back, provided the electron at site j is in $\downarrow$ state, generating $\sim \frac{t^2}{U}$ exchange. From now on

what we refer to as 'magnetic' is in context of pseudo-spins, and hence should be considered appropriately as orbital version of magnetism, for example, ferromagnetism is really a ferro-orbital order.

We use static auxiliary field (SAF) approximation [34–36], earlier applied to Hubbard model on different lattices to solve this model in real space. We use Hubbard Stratonovich transformation [37, 38] in terms of a vector field $\mathbf{m}_i(\tau)$ and a scalar field $\phi_i(\tau)$ at each site to decouple the $Un_{i\uparrow}n_{i\downarrow}$ interaction, retaining rotation invariance of the Hubbard model. We treat the $\mathbf{m}_i$ and ϕ_i as classical fields, i.e., neglect their time dependence, but completely retain the spatial fluctuations in $\mathbf{m}_i$, while we treat ϕ_i at saddle point level, i.e., $\langle\phi_i\rangle = \frac{U}{2}\langle n_i\rangle = \frac{U}{2}$ (at half filling). We have used this approach successfully in past for Mott transition on anisotropic triangular lattice [34], fcc [35] and pyrochlore [36]. Within this approximation, the model (equation (5)) maps to the following

$$H_{\text{eff}} = -t\sum_{\langle ij\rangle\alpha} a_{i\alpha}^\dagger a_{j-\alpha} - \frac{U}{2}\sum_i \mathbf{m}_i\cdot\vec{\sigma}_i + \frac{U}{4}\sum_i \mathbf{m}_i^2 \quad (6)$$

which describes the motion of electrons coupled classical auxiliary fields $\mathbf{m}_i$. The ground state of 6 is given by $\{\mathbf{m}_i\}$ that minimizes the total energy. The thermal physics is accessed using Monte Carlo (MC) sampling of the auxiliary field $\{\mathbf{m}_i\}$ that have distribution $P(\{\mathbf{m}_i\}) \propto \text{Tr}_{p,p^\dagger}e^{-\beta H_{\text{eff}}}$. We use single site update scheme, where we attempt an update $\mathbf{m}_i \to \mathbf{m}_i'$ at site $\mathbf{X}_i$. We compute the energy cost of the attempted update $\Delta E = E\{\mathbf{m}_i\} - E\{\mathbf{m}_i'\}$ by numerically diagonalizing the electronic Hamiltonian, and use Metropolis algorithm to update the auxiliary field. To access large lattices within limited time, we use travelling cluster algorithm [39] for estimating the update cost of MC, where instead of diagonalizing the full lattice, we calculate the energy cost of and update $\mathbf{m}_i$ by diagonalizing a cluster of smaller, fixed size defined with auxiliary field around the reference site. We have extensively benchmarked this cluster scheme [39]. The results we show in the next section, are averaged over equilibrium MC configurations.

3. Results

Most of our results are based on MC done on $N = 24 \times 24$ lattice, with clusters of size $N_c = 8 \times 8$, which is big enough considering finite size effects, and computational resources. We annealed the system from high temperature $T/t \approx 0.3$ for different values of U/t. We probe the magnetic correlation and transition temperature T_{corr} through thermal average of the structure factor defined as $S(q) = \frac{1}{N^2}\sum_{ij}\langle\mathbf{m}_i\cdot\mathbf{m}_j\rangle e^{i\mathbf{q}\cdot(\mathbf{R}_i-\mathbf{R}_j)}$ at each temperature. Its rapid growth at few specific $\mathbf{q}$ at some critical temperature serves us as the onset of a transition to a state with long range order, giving us an estimate of T_{corr}. Throughout the U window, the maxima of the structure factor occurs at $\mathbf{q} = (0,0)$, which describes 'ferromagnetic' order of the pseudo-spins.

The conductivity of the two dimensional system is first calculated as follows (reference [40]), using the Kubo formula:
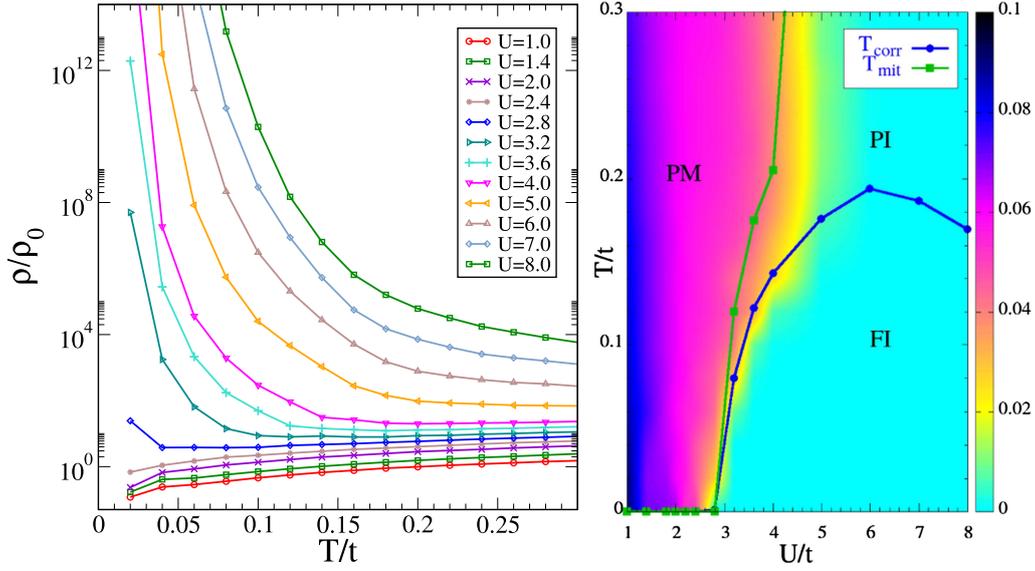
Figure 2. (Left) temperature dependence of the resistivity at different U/t. (Right) colour map of the density of state at Fermi level in U–T plane. The blue and green curves are for the magnetic transition T_{corr} and insulator metal transition, same as in figure 1 (see text).

$$\sigma^x(\omega) = \frac{\sigma_0}{N} \sum_{\alpha,\beta} \frac{n_\alpha - n_\beta}{\epsilon_{\beta\alpha}} |\langle\alpha|J_x|\beta\rangle|^2 \delta(\omega - \epsilon_{\beta\alpha}) \qquad (7)$$

$$J_x = -it \sum_{i,\vec{\delta},\sigma} \left[\vec{\delta} \cdot \hat{x} \, a^\dagger_{i,\sigma} a_{i+\vec{\delta},\sigma} - \text{h.c.}\right] \qquad (8)$$

Where, $\epsilon_{\beta\alpha} = \epsilon_\beta - \epsilon_\alpha$, J_x is current operator, and $\vec{\delta}$ runs over the set of vectors connecting the neighbouring sites. The dc conductivity is the $\omega \to 0$ limit of the above result. $\sigma_0 = \frac{\pi e^2}{\hbar}$, the scale for two dimensional conductivity, has the dimension of *conductance*. $n_\alpha = f(\epsilon_\alpha)$ is the Fermi function, and ϵ_α and $|\alpha\rangle$ are respectively the single particle eigenvalues and eigenstates of H_{eff} in a given background $\{\mathbf{m}_i\}$. The thermal average of the conductivity that we show later is averaged over equilibrium $\{\mathbf{m}_i\}$ configurations generated through MC, i.e. $\sigma(\omega, T) = \langle\langle\sigma^x(\omega)\rangle\rangle_{MC}$.

We first summarize our results in the U–T phase diagram, shown in figure 1, where the colour map represents the value of the structure factor at $\mathbf{q} = (0,0)$, indicative of ferromagnetic order. The blue curve shows the T_{corr} as function of U/t. We see that there is a critical $U_c/t \approx 3$ at $T/t = 0$, separating ferromagnetic insulator (FI) with an orbital-insensitive metal. Before U_c, we have no long range order. The T_{corr} starts to increase after U_c up to $U/t = 6$, after which it decreases monotonically (at large U/t it goes as $\sim t^2/U$). The green curve defines metal-insulator boundary $U_c(T)$, based on change of sign of resistivity derivative $d\rho/dT$.

The phases are as follows. For $U < U_c$ we have 'paramagnetic' metal (PM), characterized by increasing resistivity with temperature, and no long range spatial correlation. For $U > U_c$, we have paramagnetic insulator (PI) state at high temperature, and ferromagnetic insulator (FI) at low temperature. Both are characterized by decreasing resistivity with temperature. The T_{corr} curve (shown in blue circles in

figure 1) separates FI state with ferromagnetic order with the PI state that has no long range order.

In left panel of figure 2, we show the temperature dependence of the resistivity $\rho(T)$ at several U/t, which neatly demonstrates the MIT. At low U/t the resistivity is metallic, and increasing U/t results in progressively higher, yet metallic resistivity up to critical interaction strength $U_c/t \sim 3$, after which we have insulating resistivity, increasing with U/t.

In the metallic window of U/t, the resistivity decreases relatively slowly when T/t is lowered, while in the insulating window, the change is rather drastic due to presence of the Mott gap. The right panel of the figure 2 re-highlights the phase diagram in terms of the density of state (DOS) at Fermi level (D_{Fermi}) shown as colour map. Clearly, the insulating PI and FI phases show absence of the DOS at Fermi level, while deep in the metallic side we have non-trivial D_{Fermi}, which are close to tight-binding (TB) D_{Fermi} at low, or rather zero temperature. However, in the metallic side close to MIT, the D_{Fermi} decreases with increasing temperature. This occurs due to thermally generated auxiliary fields $\{\mathbf{m}_i\}$, which grow larger with temperature. Close to MIT line, the 'locus' of constant D_{Fermi} seems to follow the MIT line, with $D_{Fermi} \geqslant 20\%$, of its maxima, showing that the system becomes insulating before the D_{Fermi} gets depleted, or the Mott gap opens. Next, we discuss the optics and DOS.

Close to the MIT boundary on the insulating side, $U/t \approx 3.2$, the resistivity has a weak non-monotonic behaviour (figure 2 right panel). The ground state at $U = 3.2$, being close to the MIT, but on insulating side has a small gap. As the T is increased, angular fluctuations of m_i weaken the long-range order, which lowers this gap, reducing the resistivity till the gap closes. Further increase to rather large T, the magnitude fluctuations of m_i become large, which push the DOS slowly away from Fermi level. This we think results in slow increase of resistivity, and this non-monotonic behaviour. This behaviour
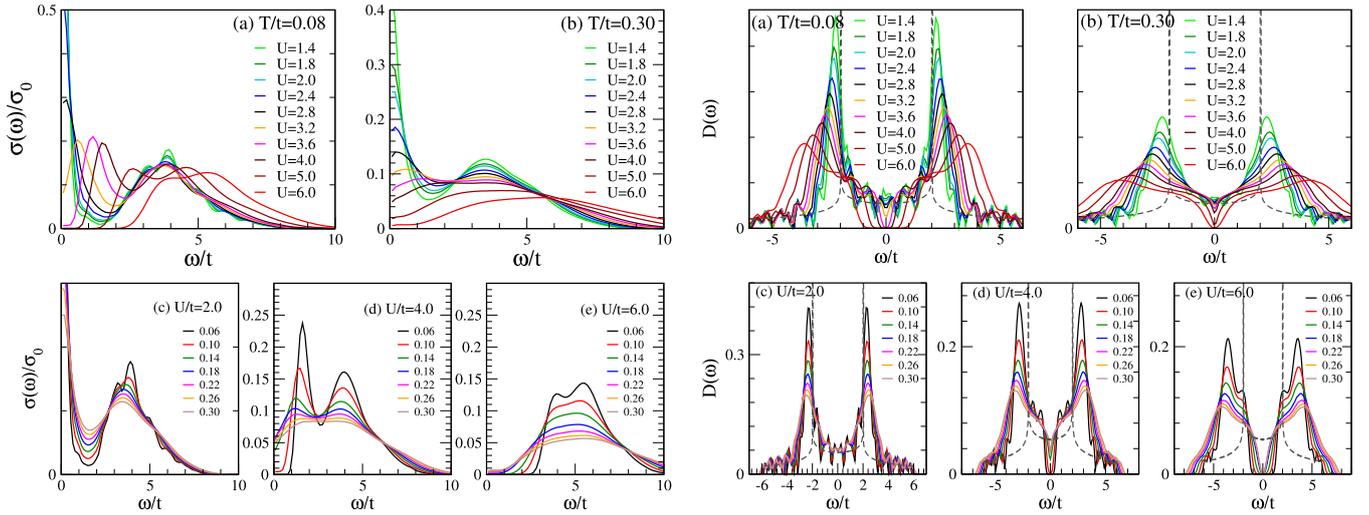
Figure 3. The left panel (a)–(e) shows optical conductivity $\sigma(\omega)$, and the right panel (a)–(e) shows the DOS. In both the panels, we show the U/t dependence at low (a) $T/t = 0.08$, and high (b) $T/t = 0.30$ temperature, while we show T/t dependence at three representative strengths of interaction (c) $U/t = 2$, (d) $U/t = 4$, (e) $U/t = 6$ (see text).

is seen close to MIT boundary, when the gap is small. The MIT boundary for Mott transition is often non-monotonic, though why it is more prominent some system than others is poorly understood.

In figure 3 we show optical conductivity (left panel), along with the DOS (right panel). Figures 3(a) and (b), show the U/t dependence of the optical conductivity (left panel) and DOS (right panel) at low $T/t = 0.08$, and high $T/t = 0.3$ temperatures. Similarly, figures 3(c)–(e) show T/t dependence of of the optical conductivity and DOS at three representative values of interaction strength (c) $U = 2$ which is metallic, (d) $U = 4$ which is insulator close to MIT, and (e) $U = 6$ deeper in insulating side. In the right panel for DOS, we also show the TB DOS in dotted line for reference.

First, the U/t dependence, at low temperature (figure 3(a), both panels). At small interaction strength U/t the low frequency Drude weight is large, as we would expect from a metal having finite DOS at Fermi level, and decreases as we move to higher U/t due to lowering of the DOS at Fermi level. The Drude weight collapses to zero as we cross to the insulating side when a gap opens in the DOS, showing a 'gapped' response at higher U/t.

In the optics, interestingly, we have a 'two-peak' behaviour at low temperature. The low energy peak is the Drude peak, which is strong at weak interaction, systematically shifts its weight from $\omega = 0$ to higher energy, to $\omega \approx mU$, m being the average magnitude of the auxiliary field $\mathbf{m}_i$, and is absent at large U/t in the insulating state. The second peak, typically prominent only in metallic side, can be attributed to the TB part of the checkerboard lattice. The TB DOS, shown in the right panel, has divergence at $\omega/t \approx \pm 2$, which would result in strong response in optical conductivity around $\omega/t \approx 4$, hence the second peak. This is what we see in the corresponding optical conductivity panel [compare (c) in both panels] when the interaction is small, system metallic, and auxiliary field magnitudes m_i dictating the spectrum are small. With increasing

interaction, the first peak progressively moves from $\omega/t = 0$, to $\omega/t \approx mU$, while the second peaks stays close to $\omega/t \approx 4$.

The divergence in the DOS, also results in making the finite size effects more severe in the metallic sides at low temperature, when auxiliary field magnitudes m_i are small, and the spectrum of the system resembles closer to that of TB system. This is seen in DOS panel, where the low temperature DOS in metallic side (c) has large fluctuations, which become smoother as one increases U [see panels (d) and (e)], or temperature.

To check the quality of our Monte-Carlo annealing, we also estimated the ground state of the equation (6) using variational minimization. We constructed spiral configurations $\mathbf{m}(\mathbf{r}) = m(\cos\mathbf{q}\cdot\mathbf{r}, \sin\mathbf{q}\cdot\mathbf{r}, 0)$ as variational states and minimized the total energy with respect to the magnitude m and period vector $\mathbf{q}$. Such periodic states can be easily diagonalized in Fourier space, as one gets only off diagonal matrix elements connecting $|\mathbf{k}\uparrow\rangle \rightarrow |\mathbf{k}+\mathbf{q}\downarrow\rangle$ and back from the $\mathbf{m}(\mathbf{r})$ dependent term. We first minimized for both $\mathbf{q}$ and m over the phase diagram on larger lattice $N = 48 \times 48$, and saw that the $\mathbf{q}$ that minimizes the energy throughout the interaction was ferromagnetic, i.e., $\mathbf{q} = (0,0)$, with U dependent $m = m_{var}$. We then calculated optimal m_{var} for ferromagnetic phase as function of U/t over even larger lattice $N = 2000 \times 2000$. In figure 4(a), we show the DOS of the variationally minimized ferromagnetic state at different U/t. In figure 4(b), we show U/t dependence of the average auxiliary field magnitude m calculated at different temperature from Monte Carlo, and compare it with the variationally minimized value m_{var}. As we see, the MC estimates of average m have non-zero values at low T and low U. This is actually consequence of MC annealing, rather than finite size, since one samples random $\mathbf{m}_i$ vectors uniformly from inside a sphere of radius, say m_0 for Monte Carlo, and one would largely generate vectors with magnitude $m > 0$, even if small, due to zero measure of point $m = 0$. Thus the MC picks up $|m| > 0$, even in the $U < U_c$ side at very low temperature. However, such issues do not occur, for example in similar
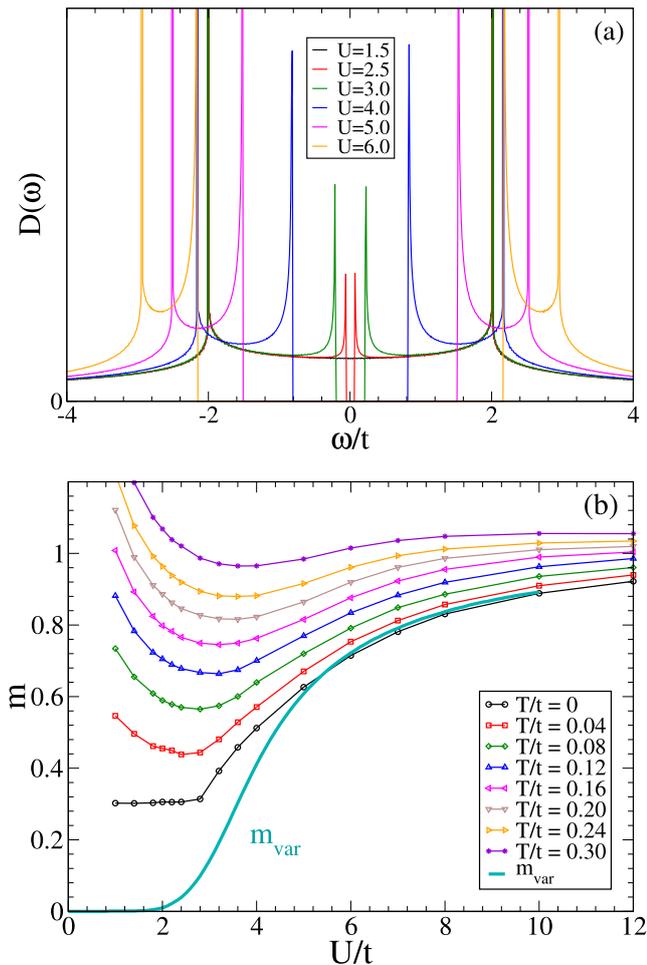
Figure 4. (a) The DOS at variationally minimized grounds state at different U/t. (b) The average magnetization m and m_{var} as function of U/t at different temperature.

simulations of say double exchange model, where the spins have unit magnitude.

At small U, when the optimal $m_{var} = 0$, we get the TB ground state, and corresponding DOS, that is nearly constant at half filling, with singularity at ± 2. Around $U \approx 2.5$, the optimal m_{var} starts growing [panel (b)], and a gap opens at half filling, and each singularity splits into two [panel (a)]. For moderate to strong interactions, $U/t \gtrsim 3$, or U_c, the average of the auxiliary field m is monotonic, i.e., it increases with U/t as well as temperature, and in large U/t limit, starts to saturate towards atomic limit. The lowest temperature MC estimate matches with the variational estimate at large interaction. At lower interaction, however, we notice that (i) the $m(U)$ profile for a given temperature is non-monotonic, and (ii) the lowest temperature m from MC is higher than the variational one. The later, results as consequence of the finite size effect, which in combination of large degeneracy in the spectrum close to and in metallic side, becomes more severe. The non-monotonicity results from the fact that at very low U, when the system's ground state is $m = 0$, finite temperature fluctuations require larger m, at smaller U, as the actual fluctuations in the spectrum depend on Um_i.

4. Discussion

We studied the complimentary scenario of weak to zero super-exchange limit, to explore the Mott transition only in term of U/t interaction window. We have done a comprehensive study of the model defined in equation (5), on checkerboard lattice, which shows strong correlation driven Mott transition with ferro-orbital order. In term of comparison with real materials, unfortunately, since majority of the pyrochlore compounds, are not half filled orbitals system with weak super-exchange, where the MIT can be seen as purely Mott phenomenon. There are ferromagnets such as $Nd_2Mo_2O_7$ and $Sm_2Mo_2O_7$ [23], but these are metals. We now comment on some limitations, and simplifications used in our model. It is worth recalling the assumption that the underlying spin-ordering remains ferro at temperatures well above orbital ordering temperature $\sim T_{corr}$ shown in figure 1. If that assumption is relaxed, say the spin-ferro ordering temperature T_c becomes comparable to the orbital T_{corr}, the core spins, of the model (equation (1)) can not be treated as frozen, and the electronic hopping becomes angle dependent. This would happen when we switch on the super-exchange interaction J_{AF}. When $J_{AF} \neq 0$, but small, the long range order of the core spins would still be ferromagnetic, however, with lower T_c. For larger J_{AF}, the ordering of the core spins would become antiferromagnetic. In either case, the electronic hopping would become angle dependent through spins (see equation (4)). One would need to include the core spins, in the simulations, as the spin fluctuations driven hopping would crucially impact electronic properties, including transport. As a result, the effective electronic delocalisation would reduce, pushing the Mott boundary to lower values, along with possibly reducing the T_{corr} scales. As mentioned above, for large J_{AF}, more accurate treatment would require solving the current model with spin dependent hopping, and we plan to present such a work separately in future.

We considered only the inter-orbital hopping in the current work, which led to ferro-orbital order. However in reality, the intra-orbital hopping would also be non-zero. To understand its impact, consider the two limits, (i) the spin conserving limit, $t_{\alpha \neq \beta} = 0$, the effective exchange between sites as seen at half filling through virtual hopping is AF with exchange $\sim t^2/U$ at large U. (ii) With spin conserving term being zero, $t_{\alpha = \beta} = 0$, where the corresponding exchange is ferro due to alternating hopping. When both hoppings are present and comparable, so are the corresponding competing exchanges, which would lead to emergence of other long-range orders. Such scenario, even without the complications of super-exchange, is an intriguing test bed of frustration in orbital space, and warrants further investigation.

We also wish to comment on phase diagram near the Mott transition, in figure 2 (right), where we plot the MIT boundary, the T_{corr} curve, and DOS at Fermi level as colour. The Mott transition, usually reflects a windows of pseudo-gap at finite temperature [34, 36], bracketing the MIT curve. Our coloured DOS with colour values between 20% to upto $\approx 50\%$ represents a rough estimate of the pseudo-gap window.

5. Conclusion

We studied correlation driven orbital Mott transition in two dimensional pyrochlore lattice using a real space based Monte Carlo approach, and established finite temperature phase diagram describing the Mott transition, in terms of MIT boundary, orbital ordering, and a rough estimate of pseudo-gap window. We also calculated electronic transport, optical conductivity, and thermal density of states across the Mott transition.

Acknowledgments

ORCID iDs

Rajarshi Tiwari https://orcid.org/0000-0002-1209-3502

References

[1] Mott N F 1949 *Proc. R. Soc.* A **62** 416
[2] Mott N F 1990 *Metal-Intulator Transitions* (London: Taylor and Francis)
[3] Imada M, Fujimori A and Tokura Y 1998 *Rev. Mod. Phys.* **70** 1039
[4] Streltsov S V and Khomskii D I 2017 *Phys.-Usp.* **60** 1121
[5] Chen H 2018 *npj Quantum Mater.* **3** 57
[6] Rong Y and Si Q 2012 *Phys. Rev. B* **86** 085104
[7] Florens S, Georges A, Kotliar G and Parcollet O 2002 *Phys. Rev. B* **66** 205102
[8] Kita T, Ohashi T and Kawakami N 2011 *Phys. Rev. B* **84** 195130
[9] De Franco C, Tocchio L F and Becca F 2018 *Phys. Rev. B* **98** 075117
[10] Grandi F, Amaricci A, Capone M and Fabrizio M 2018 *Phys. Rev. B* **98** 045105
[11] Georges A, Kotliar G, Krauth W and Rozenberg M J 1996 *Rev. Mod. Phys.* **68** 13
[12] Park H, Haule K and Kotliar G 2008 *Phys. Rev. Lett.* **101** 186403
[13] Kajueter H and Gabriel K 1997 *Int. J. Mod. Phys.* B **11** 729–51
[14] de Medici L, Hassan S R, Capone M and Dai X 2009 *Phys. Rev. Lett.* **102** 126401
[15] Koga A, Kawakami N, Rice T M and Sigrist M 2004 *Phys. Rev. Lett.* **92** 216402
[16] Maier T, Jarrell M, Pruschke T and Hettler M H 2005 *Rev. Mod. Phys.* **77** 1027
[17] Sato T, Hattori K and Tsunetsugu H 2012 *Phys. Rev. B* **86** 235137
[18] Gardner J S, Gingras M J P and Greedan J E 2010 *Rev. Mod. Phys.* **82** 53
[19] Motome Y and Furukawa N 2011 *J. Phy.: Conf. Ser.* **320** 012060
[20] Matsuhira K, Wakeshima M, Hinatsu Y and Takagi S 2011 *J. Phys. Soc. Jpn.* **80** 094701
[21] Nakatsuji S, Machida Y, Maeno Y, Tayama T, Sakakibara T, van Duijn J, Balicas L, Millican J N, Macaluso R T and Chan J Y 2006 *Phys. Rev. Lett.* **96** 087204
[22] Ueda K, Fujioka J, Takahashi Y, Suzuki T, Ishiwata S, Taguchi Y and Tokura Y 2012 *Phys. Rev. Lett.* **109** 136402
[23] Iguchi S, Hanasaki N, Kinuhara M, Takeshita N, Terakura C, Taguchi Y, Takagi H and Tokura Y 2009 *Phys. Rev. Lett.* **102** 136407
[24] Hanasaki N, Watanabe K, Ohtsuka T, Kezsmarki I, Iguchi S, Miyasaka S and Tokura Y 2007 *Phys. Rev. Lett.* **99** 086401
[25] Fritsch K, Ross K A, Qiu Y, Copley J R D, Guidi T, Bewley R I, Dabkowska H A and Gaulin B D 2013 *Phys. Rev. B* **87** 094410
[26] Fujimoto S 2003 *Phys. Rev. B* **67** 235102
[27] Ishizuka H, Udagawa M and Motome Y 2011 *Phys. Rev. B* **83** 125101
[28] Carter J-M and Kee H-Y 2013 *Phys. Rev. B* **87** 014433
[29] Disseler S M, Giblin S R, Dhital C, Lukas K C, Wilson S D and Graf M J 2013 *Phys. Rev. B* **87** 060403(R)
[30] Motome Y and Furukawa N 2010 *Phys. Rev. Lett.* **104** 106407
[31] Solovyev I V 2003 *Phys. Rev. B* **67** 174406
[32] Ichikawa H *et al* 2005 *J. Phys. Soc. Jpn.* **74** 1020
[33] Moritomo Y, Xu S, Machida A, Katsufuji T, Nishibori E, Takata M, Sakata M and Cheong S-W 2001 *Phys. Rev. B* **63** 144425
[34] Tiwari R and Majumdar P 2014 *Eur. Phys. Lett.* **108** 27007
[35] Tiwari R and Majumdar P 2013 arXiv:1302.2922
[36] Swain N, Tiwari R and Majumdar P 2016 *Phys. Rev. B* **94** 155119
[37] Schulz H J 1990 *Phys. Rev. Lett.* **65** 2462
[38] Hirsch J E 1983 *Phys. Rev. B* **28** 4059
[39] Majumdar S K P 2006 *Eur. Phys. J. B* **50** 571
[40] Allen P B 2006 *Conceptual Foundation of Materials V.2,* ed S G Louie and M L Cohen (Amsterdam: Elsevier)